

Probing the radiation-dominated regime of laser-plasma interaction in multi-beam configurations of petawatt lasers

T.V. Liseykina*

*Institute of Computational Mathematics and Mathematical Geophysics SB RAS
Lavrentiev ave. 6, Novosibirsk, 630090, Russia*

E.E. Peganov†

National Research Nuclear University MEPhI, Kashirskoe shosse 31, 115409, Moscow, Russia

S.V. Popruzhenko‡

*National Research Nuclear University MEPhI, Kashirskoe shosse 31, 115409, Moscow, Russia and
Prokhorov General Physics Institute RAS, Vavilova 38, 119991, Moscow, Russia*

(Dated: September 13, 2024)

We model numerically the ultrarelativistic dynamics of a dense plasma microtarget in a focus of several intersecting femtosecond laser pulses of multi-petawatt power each. The aim is to examine perspective future experimental approaches to the search of the Inverse Faraday Effect induced by radiation friction. We show that multi-beam configurations allow lowering the peak laser power required to generate a detectable quasi-static longitudinal magnetic field excited due to the radiation reaction force. The effect remains significant at angles around 10° between the beams, vanishes when the angle exceeds 20° , and remains rather stable with respect to variations of relative phases and amplitudes of the beams. We conclude that using four infrared femtosecond linearly polarized pulses, 15 petawatt power each, crossing at angles $\approx 10^\circ$, the radiation-dominated regime of laser-plasma interaction can be experimentally demonstrated.

Keywords: intense laser radiation, laser-plasma interaction, radiation reaction, Inverse Faraday Effect, magnetic fields

I. INTRODUCTION

Effects of radiation friction or, equivalently, the radiation reaction force in dynamics of charged particles, beams and plasma subject to intense electromagnetic fields have remained in the scope of interest of strong-field physics for several latest decades. Recently physics of the radiation reaction force (RRF) has become even more topical, thanks to the considerable progress in design and construction of multi-petawatt laser sources potentially capable to produce ultrashort electromagnetic pulses of intensity $10^{23}\text{W}/\text{cm}^2$ and higher (see reviews [1–3] for information on the current status of high-power laser facilities). The theoretical framework for treatment of the RRF in classical electrodynamics has been amply developed [4, 5] in the past, and various signatures of radiation reaction in the dynamics and radiation of fast particles in external fields such as radiation damping in accelerators or radiation losses for cosmic rays had become tutorial examples. However, the subject remains topical and essentially intricate because of the two circumstances raising at the overlap of plasma physics and that of extreme electromagnetic fields. Firstly, in a dense plasma driven by extremely strong electromagnetic fields of short focused laser pulses, the RRF is expected to alter

the collective dynamics providing conditions for a new interaction regime called *radiation-dominated dynamics* and enriched by new mechanisms of particle acceleration and magnetic fields generation. Secondly, applying intensities above $10^{24} - 10^{25}\text{W}/\text{cm}^2$ or using pre-accelerated plasma interacting with pulses of lower intensity one may enter the quantum regime of radiation reaction, whose theoretical understanding remains incomplete [6]. Experiments in this intensity domain can provide fundamental knowledge useful for the development of a comprehensive quantum theory of radiation reaction. For the detailed description of this research field, which currently remains dominated by theory with just a few experimental demonstrations of RRF reported so far [6–8], we send the reader to reviews [1–3, 9, 10] and the literature quoted therein.

The Inverse Faraday effect (IFE) [11–13] induced by the RRF in collisionless plasma interacting with circularly polarized (CP) electromagnetic radiation of extreme intensity can serve as an example of such collective plasma phenomenon arising due to radiation friction [14–16]. The IFE provides a new mechanism for the excitation of strong quasi-static magnetic fields in plasma, and, more importantly, it can be used as a benchmark of the radiation-dominated dynamics in classical or quantum regimes of laser-plasma interactions. It was shown in Ref.[14] that the synchrotron-like emission by fast electrons in a CP laser pulse results in a considerable irreversible angular momentum transfer from the field to the plasma followed by the excitation of ring-like electron currents in the polarization plane, which in turn gen-

* Correspondence email address: tatiana.liseykina@gmail.com

† Correspondence email address: egor.peganov@gmail.com

‡ Correspondence email address: sergey.popruzhenko@gmail.com

erate a quasi-static magnetic field. At laser intensities $\simeq 10^{24}\text{W}/\text{cm}^2$, this magnetic field can reach an amplitude of several giga-Gauss (GG). More precisely, for the interaction of a CP pulse of $\lambda = 800\text{nm}$ wavelength and a super-Gaussian lateral intensity distribution of width $r_0 = 3.8\lambda$ the generation of a 1 GG magnetic field was predicted in the simulation [14] for the peak intensity $J = 4.4 \cdot 10^{23}\text{W}/\text{cm}^2$. The magnetic field exists for more than 100 fs in the volume $\simeq 50\lambda^3$ and should be accessible for detection by proton diagnostics.

The aforementioned parameters require the peak laser intensity $\approx 80\text{PW}$ at $\approx 1.2\text{kJ}$ pulse energy. But despite the significant advances in petawatt (PW) laser technologies demonstrated in the two past decades, such parameters are still far from reach in laboratories. The peak power of 10-15 PW at a pulse duration 20-30 fs looks as an optimistic promise for the nearest future. The corresponding energies are 100-300 J per pulse. Several laser facilities [17–21] are filling currently the interval of 1-10 PW power. With this power level secured, projects of multibeam sub-exawatt laser installations will become realistic. The laser facility XCELS combining up to 12 synchronized 10-15 PW laser beams can serve an example of such projects [22], which can be put in realization within the nearest decade.

The possibility to superimpose coherently several laser beams in the focal area will allow lowering the power and pulse energy thresholds required to achieve the radiation dominated regime, including the generation of strong magnetic fields through the IFE. The multi-beam scheme would also eliminate the necessity of converting an initially linearly polarized (LP) beam into a CP one as it will be sufficient to use several pairs of LP beams with mutually orthogonal polarizations propagating at small angles to each other. In this work, we examine such a scheme numerically by modeling the laser-plasma interaction within the particle-in-cell (PIC) method using the codes UMKA [23–25] and SMILEI [26]. We aim at the following objectives: (a) to estimate the minimal laser power and pulse energy required for the generation of a significant, detectable magnetic field due to the radiation reaction effect in a multi-beam configuration and (b) to check the sensibility of the generated magnetic field peak amplitude and spatial distribution to the relative phase shifts of the beams, variations in their amplitudes and to the angle at which the beams intersect. The robustness of the scheme with respect to the first two factors is of particular importance, since they are difficult to control in multi-PW sources with a low repetition rate. The angle between the beams' propagation directions needs optimization because the electromagnetic field structure close to CP vanishes quickly with this angle increasing, while using nearly parallel beams intersecting at small angles is technically difficult. The output of our study will help to formulate requirements to the architecture of multi-beam multi-PW laser source XCELS and other laser facilities of similar class.

The structure of the paper is following. In the next

section II we formulate the statement of the problem and discuss parameters of the laser pulses and plasma. Section III is dedicated to presentation and discussion of numerical results. Section IV presents conclusions and outlook. Preliminary results of our calculations related to the two-beam scheme were reported in [27].

II. STATEMENT OF THE PROBLEM

A. Interaction scheme and parameters

We consider the interaction of two or four LP laser beams of $\lambda = 800\text{nm}$ wavelength with a helium fully pre-ionized plasma slab of a 10λ thickness and initial concentration $n_0 = 1.55 \times 10^{23}\text{cm}^{-3} = 90n_c$ with

$$n_c = \frac{m_e \omega^2}{4\pi e^2} \quad (1)$$

being the critical concentration for the laser frequency $\omega = 2\pi c/\lambda$; m_e and e are the electron mass and elementary charge correspondingly. We characterize the electromagnetic field amplitude E_0 by its invariant dimensionless form

$$a_0 = \frac{eE_0}{m_e c \omega} \quad (2)$$

with c being the speed of light. A position-dependent analog $a(\mathbf{r})$ of (2) is defined by replacing the field amplitude E_0 with $E(\mathbf{r}) = \sqrt{\langle E^2 \rangle(\mathbf{r})}$, where $\langle \dots \rangle$ denotes time averaging. The plasma parameters are chosen to keep them close to a set of earlier calculations [14–16], where we studied the IFE in a single CP beam of intensity $J \approx 10^{24}\text{W}/\text{cm}^2$ and higher. For LP pulses of frequency $\omega = 2.4 \cdot 10^{15}\text{s}^{-1}$, $a_0 = 1$ at $J = 2.1 \cdot 10^{18}\text{W}/\text{cm}^2$. In a single CP laser beam, our previous calculations [14, 15] did not reveal any significant longitudinal magnetic field for $a_0 < 200$. Thus in the present calculation we are interested in intensities $\approx 8 \cdot 10^{22}\text{W}/\text{cm}^2$ in a single beam.

We consider laser pulses ejected through the left boundary of the simulation box. This is achieved through a time-dependent boundary condition set on the $x = -5\lambda$ plane. The finite-difference time-domain method [28, 29] with the total-field/scattered field formulation [30] in x -direction is used to propagate the electromagnetic fields. To obtain the distributions of the magnetic field strength \mathbf{B}_\perp on the left boundary we consider a super-Gaussian beam [31] of the following form

$$\mathbf{B}_\perp = E_0 \mathbf{p} \exp \left\{ -\frac{(y'^2 + z'^2)^2}{r_0^4} - \frac{(x' - ct)^4}{r_c^4} \right\} \times \begin{pmatrix} \cos(kx' - \omega t) \\ \sin(kx' - \omega t) \end{pmatrix}. \quad (3)$$

Here E_0 is the electric and magnetic peak field amplitude in (2) and \mathbf{p} is the field polarization vector. Coordinates (x', y', z') in (3) are introduced for each beam

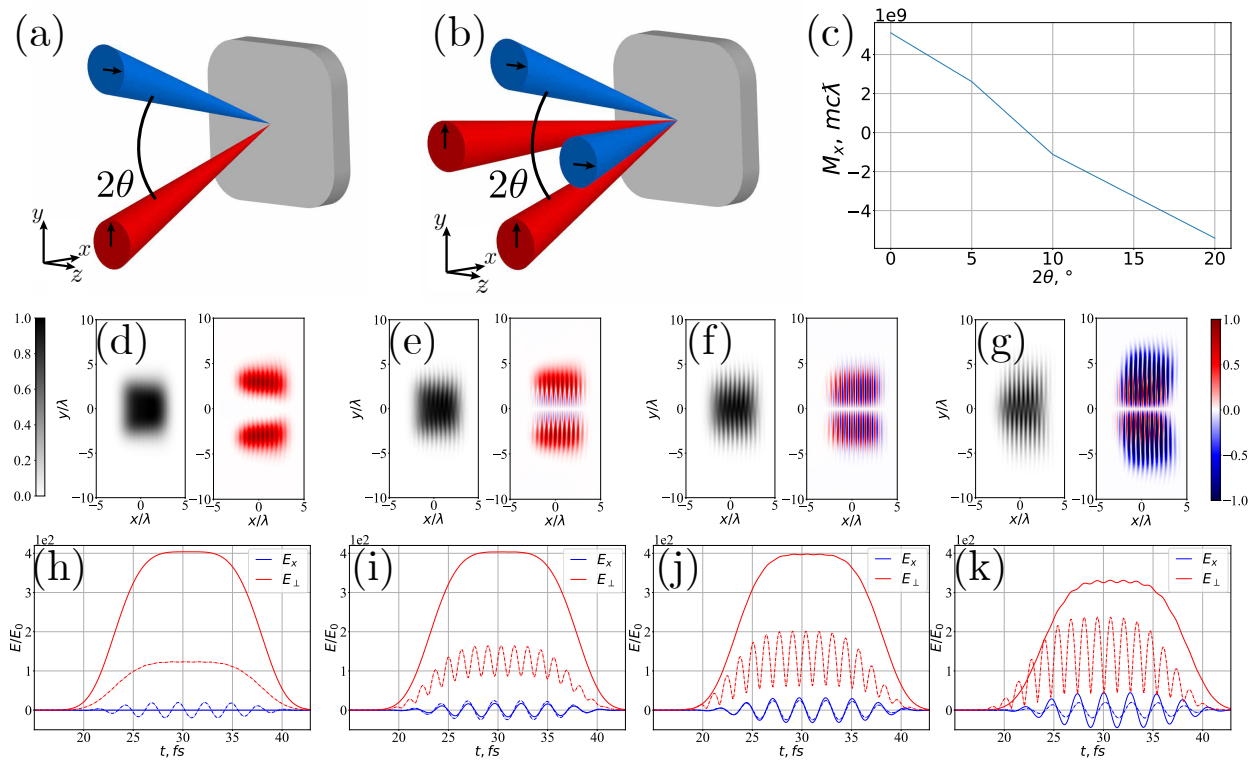


FIG. 1. First row: sketch of the 2-beam (a) and 4-beam (b) setups; projection of the total angular momentum M_x of the laser field on the axis x perpendicular to the plasma slab as function of θ for the 4-beam case. The angular momentum is measured in units of $mc\lambda \approx 2.5 \cdot 10^{22} \text{erg} \cdot \text{s}$ (c). Second row: instant distributions in $a^2(x, y)$ (left panels, gray-scale) and m_x (right panels, color-scale) for $2\theta = 0^\circ$ (d), $2\theta = 5^\circ$ (e), $2\theta = 10^\circ$ (f) and $2\theta = 20^\circ$ (g) for the 4-beam case. Each distribution is normalized to the maximum value of the plotted quantity. Third row: time dependence of E_x (blue lines) and $E_\perp = \sqrt{E_y^2 + E_z^2}$ (red lines) at points $(0, 0, 0)$ (solid lines) and $(0, 4\lambda, 0)$ (dash-dotted lines) for the same set of angles as in the second row.

individually such that the wave vectors $\mathbf{k}' = (k, 0, 0)$ are orthogonal to the corresponding (y', z') planes. Primed coordinates are related to laboratory ones used in the simulation by rotation through an angle θ in the (x, y) plane for the two-beam setup and in the (x, y) and (x, z) planes for the four-beam setup. Schematic representation of both setups is shown on Fig. 1(a,b). The beam lateral waists and the longitudinal pulse lengths are taken $r_0 = 3.8\lambda$ and $r_c = 3\lambda$ correspondingly. The effective pulse duration is $\tau = 3\lambda/c = 6\pi/\omega \approx 7.2$ fs. This is roughly 3 times shorter than a typical pulse duration for most of the multi-PW sources. This difference is not of crucial importance for our analysis, while the application of such short pulses considerably accelerates demanding numerical simulations.

The applied boundary condition (3) does not focus the field on the plasma surface, instead the beams appear at $x = 0$ defocused compared to the plane $x = -5\lambda$. This defocusing is relatively weak thanks to small distance between the boundary and the plasma surface. Thus the peak intensity estimated using of the field distribution (3) on the boundary does not differ much from the value reached on the plasma slab surface. Solutions found in free space (without plasma) allow to check, how quickly

the field in the area where the beams overlap starts deviating from CP with the angle θ increasing. We characterize this deviation by the distributions in dimensionless intensity $\tilde{J} = a_0^2(\mathbf{r})$ and in the density of x-projection of angular momentum $\mathbf{m}(\mathbf{r}) = [\mathbf{r}[\mathbf{E}\mathbf{B}]]/4\pi c$ shown in Fig. 1(d-g). For a CP beam the a^2 -distribution is smooth (Fig. 1(d)), and the m_x density is everywhere positive, while for $\theta \approx 10^\circ$ a considerable difference is already clearly seen. The sign of the integrated projection M_x flips at $2\theta \approx 10^\circ$ (Fig. 1(c)). The time dependence of the electric field projection E_x and of the absolute value of its lateral component $E_\perp = \sqrt{E_y^2 + E_z^2}$ shown in panels of Fig. 1(h-k) also demonstrates the deviation from CP increasing with the growth of the convergence angle. For $2\theta > 10^\circ$ the field structure remains close to CP on the axis $y = z = 0$, while at $y = 4\lambda$ the deviation is apparent. Taking into account that the IFE is induced by electron currents excited near the laser beam lateral edge ($\approx 3 - 4\lambda$ in our case) [14] this deviation should considerably suppress the magnetic field generation. Our further simulations (not present in the plot) show that the field structure in the overlap area of the beams depends on the boundary condition. In particular, a Gaussian

boundary condition such that the beams overlap in their focal waists leads to a slower decrease in the degree of CP with θ increasing. However, this does not change our results qualitatively. Summarizing the information delivered in Fig. 1, we conclude that with θ increasing, the field structure in the focus deviates from CP rather quickly so that the case $\theta > 10^\circ$ is not of interest for the detection of IFE signatures [27].

Numerical runs described in the next subsection were arranged such that the time instant $t = 0$ is that one when the laser pulse front edge arrives to the front surface of the plasma slab at $x = 0$ so that $t > 0$ is time past after the start of the interaction. With the efficient pulse duration $\tau = 3T_L \approx 7.2\text{fs}$ the laser field is being entirely reflected by the plasma during $\tau_{\text{int}} \approx 15 - 20\text{fs}$, which can be considered as the full interaction time. We look at the magnetic field excited in the plasma after the interaction, typically at $t = 30 - 40T_L$. For the super-Gaussian pulse (3) the peak power is

$$P = \frac{\pi^{3/2}}{2\sqrt{2}} J_0 a_0^2 r_0^2 \quad (4)$$

with $J_0 = 2.1 \cdot 10^{18}\text{W/cm}^2$ for $\lambda = 800\text{nm}$ and LP. Taking $a_0 = 200$ one obtains from (4) $P \approx 16\text{PW}$, the value close to that expected at the XCELS laser facility under development [22]. The full pulse energy is about 150W. Note that (4) only gives an estimate of the peak laser power, because the field structure in the interaction volume obtained through the numerical solution of the Maxwell equations deviates considerably from (3).

B. Numerical methods

The interaction scenario described above was numerically modeled using two independently developed PIC codes UMKA [23–25] and SMILEI [26]. The two codes provide similar though not identical results for the number of nodes not less than 32 per laser wavelength and a sufficiently large number of macroparticles per cell.

In the simulations, 64 macroions and macroelectrons per cell were used at the spatial resolution $\Delta x, \Delta y, \Delta z = \lambda/40$. Boundary conditions for the fields on the left plane of the computational domain, $x = -5\lambda$, are given by (3). Otherwise, the conditions for the fields and particles are: absorption in the propagation direction and periodicity in the lateral directions. The size of the simulation box $[35 \times 25 \times 25]\lambda^3$ is chosen sufficiently large to rule out any boundary effects on the particles' and fields' distributions in the central part of the simulation domain.

In both codes, the radiation reaction force \mathbf{F}_{RR} is included in the equations of motion for electrons in the form [4]

$$\mathbf{F}_{RR} = -\frac{2}{3}r_e^2 \left[\gamma^2 \left(\mathbf{F}_L^2 - \left(\frac{\mathbf{v}}{c} \cdot \mathbf{E} \right)^2 \right) \frac{\mathbf{v}}{c} - \mathbf{F}_L \times \mathbf{B} - \left(\frac{\mathbf{v}}{c} \cdot \mathbf{E} \right) \mathbf{E} \right]. \quad (5)$$

Here, $r_e = e^2/mc^2 \approx 2.8 \times 10^{-13}\text{cm}$ is the classical electron radius, \mathbf{v} is the electron velocity, $\mathbf{F}_L = (\mathbf{E} + \mathbf{v}/c \times \mathbf{B})$ and $\gamma = 1/\sqrt{1 - v^2/c^2}$ is the relativistic gamma-factor. This is a reduced expression for the RRF, compared to its full Landau-Lifshitz form [4]. It follows from the latter after omitting terms (small in the considered case) containing time and space derivatives of the electromagnetic fields. Note that here we treat radiation reaction classically, which is amply sufficient for the considered parameters of the laser pulses. For account of quantum effects in descriptions of the RRF and in particular of the IFE, see reviews [2, 10] and papers [16, 32–34]. The codes use a numerical algorithm based on the assumption that the acceleration of particles in their rest frame is dominated by the Lorentz force (see Ref. [35] for detail). The numerical implementation allows adding radiation reaction effects to any PIC code based on the standard Boris pusher algorithm for the calculation of the particles acceleration with small computational costs.

Inclusion of dissipative radiation losses through the RRF in a PIC code is justified if the following conditions are met: 1) characteristic frequencies of synchrotron-like radiation emitted by the plasma electrons are much higher than the highest frequency that can be resolved on the numerical grid; 2) radiation at such frequencies is incoherent; 3) the plasma is transparent for electromagnetic fields of these frequencies. For the present calculations, these requirements are well satisfied (see estimates in Refs.[14, 16]). At lower though still ultra-relativistic intensities, radiation responsible for the RRF may become partially coherent, which requires to revisit the description of radiation reaction effects. For this specific case, see recent publications [36, 37].

III. RESULTS AND DISCUSSION

Our discussion is centered around magnetic field distributions in space for (a) different number of the beams, (b) different angles of convergence θ and (c) the case of fluctuations in relative phases and amplitudes of the beams. All distributions shown in plots correspond to the time instant $t = 35T_L \approx 85\text{fs}$ after the beginning of the interaction, i.e. more than 50fs after the laser pulse is reflected.

Firstly, we examine the efficiency of the magnetic field excitation in different geometries. To this end, we compare the distributions of the longitudinal magnetic field B_x recorded at $t = 35T_L$ for the 2- and 4-beam cases at different convergence angles. The magnetic field amplitude is normalized to $B_0 = m_e c \omega / e = 1.38 \cdot 10^8 \text{Gauss}$. To reduce fluctuations and make the signal smoother, we integrate the distributions over angle in the (y, z) plane so that the field B_x in Fig. 2 depends on the longitudinal coordinate x and the radial one $r = \sqrt{y^2 + z^2}$.

From these distributions, we gain that:

1. When the IFE is present for collinear beams, it survives for the angles of convergence up to $2\theta \simeq 10^\circ$.

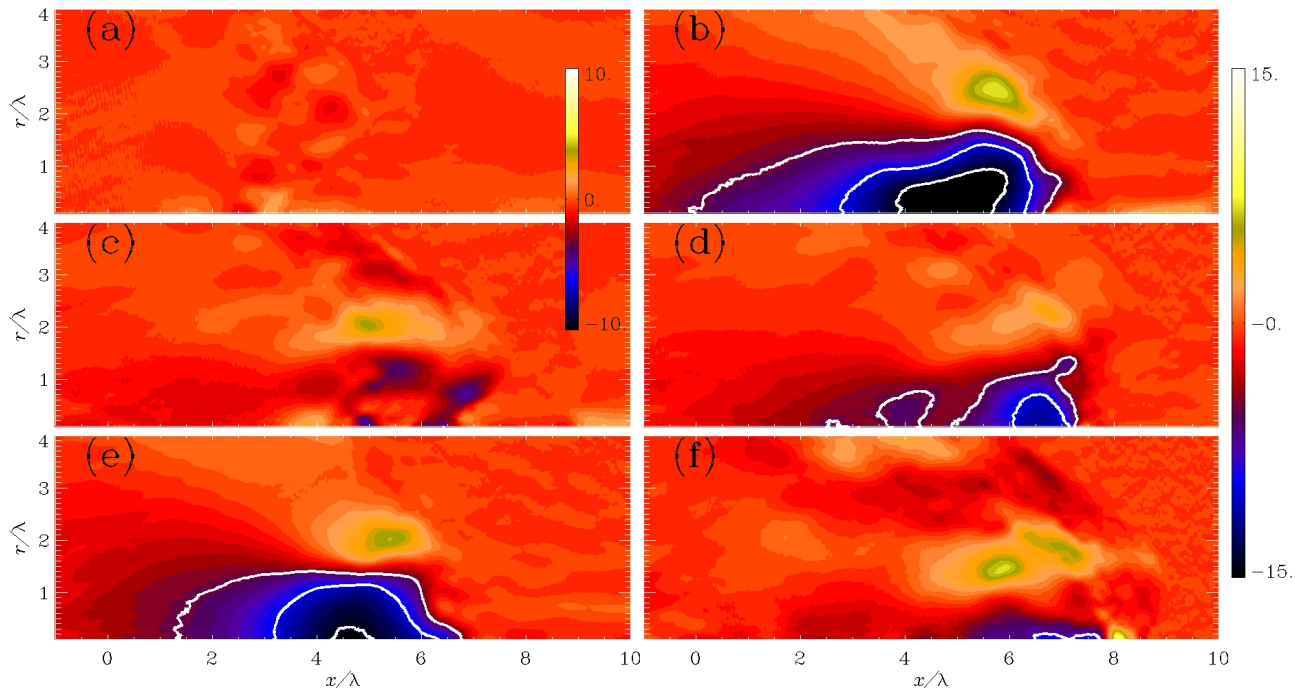


FIG. 2. Spatial distributions in B_x/B_0 as functions of x and $r = \sqrt{y^2 + z^2}$ at $t = 35T_L$ for the cases of two (a,c) and four (b,d,f) beams with the angle of convergence (see Fig. 1 and text around for explanations) $2\theta = 5^\circ$ (a), (b); $2\theta = 10^\circ$ (c), (d) and $2\theta = 20^\circ$ (e), (f). The single beam power was fixed by 16PW corresponding to $a_0 = 200$. For reference, panel (e) shows the distribution for a single CP beam with power $P = 64\text{PW}$ equal to the total power of the four beams. Panel (c) gives the distribution for the same case as (a), but assuming 32PW ($a_0 = 280$) in each beam instead of 16 PW. Note different color scales in panels (a,c) and (b,d,e,f) correspondingly. The lines of constant magnetic field $B_x = [-15, -10, -5]B_0$ are displayed white.

For $2\theta \simeq 20^\circ$ the magnetic field drops down considerably, both in the amplitude and the size of space where the magnetic field is present. These features are similar for 2 and 4 beams. For the 2-beam scheme a similar behavior was reported in a brief publication [27].

2. The difference between the 2- and 4-beam schemes is evident for the fixed power of a single beam. The distributions of Fig. 2(a,c) show that for the 2-beam scheme the threshold power, when some signatures of the magnetic field generated through the IFE can be expected, is $\simeq 30\text{PW}$, well above the presently achieved level of 5PW and the soon expected that of 15PW. Instead, the 4-beam scheme should work reliably at the 15PW power. For the scale $B_x \in [+10, -10]B_0$ of panels (a) and (c) no magnetic field is visible when two 15PW beams are applied. Reduction of the interval reveals some fields B_x which however lie beyond the reliable signal level of the present PIC simulations.
3. The quasi-static longitudinal magnetic field B_x vanishes in correlation with the decrease in the longitudinal projection of the field angular momentum (see Fig. 1), which agrees well with macroscopic picture of the IFE [14] based on the irreversible transfer of angular momentum from the field to the

particles. However, one can notice from the comparison of Fig. 1(c) and Fig. 2 (d,f) that the magnetic field of negative sign survives even when the sign of M_x is changed. An explanation of this extended survival of the IFE with the angle between the beams increasing stems from the distributions shown in Fig. 1(f,g) and (h-k). It is clear from these plots that the density of m_x remains positive in the central part of the interaction volume, up to $r \approx 3\lambda$, while the electron current generating the field is concentrated near $r \approx 2\lambda$. The lateral electric field although oscillates at $y = 4\lambda$, still contains a significant fraction of a CP component. The periphery of the interaction volume, which contributes a lot into the net angular momentum M_x still plays a minor role in the excitation of the electron current.

Secondly, for multi-PW laser sources with sub-kJ pulse energies and low repetition rates, it is hard to expect the beams to be well synchronized in phase and amplitude. For such laser systems under development, the option of fully incoherent beams is also considered as one of realistic scenarios. Thus it is of high relevance for the future experiments to make a step out of the idealistic assumption of fully coherent in-phase beams and to study sensibility of the effect to the fluctuations of relative phases and amplitudes of the beams. Fig. 3 presents the magnetic field distribution $B_x(r, x)/B_0$ recorded at $t = 35T_L$

for the 4-beam case with $2\theta = 5^\circ$ and $2\theta = 10^\circ$. These cases were chosen basing on the analysis of the distributions present in Fig. 2. Panels (a-f) correspond to regular phase shifts between the pairs of beams with orthogonal polarizations, i.e. between the two blue and the two red beams in Fig.1(b), while (g) and (h) show the distributions generated by beams with randomly shifted phases and amplitudes, correspondingly.

As expected, the efficiency of the magnetic field generation drops down with the phase shift increasing. This suppression can be qualitatively demonstrated by plotting contours of the constant magnetic field for different phase shifts. The result is shown in Fig. 4. It is important to note that the effect survives in a broad interval of relative phases. Comparison of panels (c), (d) (e) and (f) in Fig. 3 shows that the magnetic field remains visible at relative phases filling more than 50% of the interval $(0, \pi/2)$. The distributions in Figs.3 and 4 were calculated for higher field amplitudes $a_0 = 250$ and $a_0 = 500$. In the latter case, the 2-beam scheme was considered. A comparison of results presented in these Figures shows, in particular, that both the schemes are, on the qualitative level, equally sensitive to fluctuations of relative phases of the beams. In experiment, both the relative phases and amplitudes of the beams will fluctuate. Panels (g) and (h) of Fig.3 show the distributions for randomly chosen phase shifts and amplitudes. These results also suggest that the scheme is acceptably stable with respect to these parametric uncertainties.

IV. CONCLUSION

In conclusion, we have studied the possibility to reach the radiation-dominated regime of the laser plasma in-

teraction and, in particular, to observe the Inverse Faraday effect driven by radiation reaction in a multi-beam scheme. Our numerical results show that application of four beams partially synchronized in phase and amplitude lowers the single beam power required for reliable detection of the quasi-static longitudinal magnetic field excited through the IFE to 15 PW, which looks a realistic value for several forthcoming laser facilities. Most importantly, the effect is shown rather robust with respect to fluctuations of relative phases and amplitudes. This enhances the possibility of observation at low repetition rates typical for multi-PW laser sources. At the future XCELS facility [22] installations with up to 12 beams are considered. From one side, increasing the number of beams will obviously further lower the power threshold required for IFE observation. From the other side, taking into account the constraints on the angle θ and the relative phase shifts we formulated in this paper, application of ~ 10 or more beams may appear highly problematic from the technical viewpoint. We conclude that the 4-beam scheme at the 10–15PW level is optimal for the search of the giant magnetic field excitation in the radiation-dominant regime.

ACKNOWLEDGMENT

Numerical simulations were performed at the Joint Supercomputer Center of the Russian Academy of Sciences and the Computing Center at the MEPHI Laboratory for Extreme Light Physics. EEP acknowledges support from the Ministry of science and higher education (agreement No.075-15-2021-1361 signed on 07.10.2021). TVL and SVP acknowledge support of the Russian Science Foundation (grant No. 20-12-00077).

-
- [1] A. Gonoskov, T. Blackburn, M. Marklund, and S. Bulanov, *Reviews of Modern Physics* **94**, 045001 (2022).
 - [2] A. Fedotov, A. Ilderton, F. Karbstein, B. King, D. Seipt, H. Taya, and G. Torgrimsson, *Physics Reports* **1010**, 1 (2023).
 - [3] S. V. Popruzhenko and A. M. Fedotov, *Phys. Usp.* **66**, 460 (2023).
 - [4] L. Landau and E. Lifshitz, *Theoretical physics. Field theory* (Nauka, 1967).
 - [5] J. D. Jackson, *Classical electrodynamics* (John Wiley & Sons, 2021).
 - [6] A. Macchi, *Physics* **11**, 13 (2018).
 - [7] J. Cole, K. Behm, E. Gerstmayr, T. Blackburn, J. Wood, C. Baird, M. J. Duff, C. Harvey, A. Ilderton, A. Joglekar, *et al.*, *Physical Review X* **8**, 011020 (2018).
 - [8] K. Poder, M. Tamburini, G. Sarri, A. Di Piazza, S. Kuschel, C. Baird, K. Behm, S. Bohlen, J. Cole, D. Corvan, *et al.*, *Physical Review X* **8**, 031004 (2018).
 - [9] G. A. Mourou, T. Tajima, and S. V. Bulanov, *Reviews of modern physics* **78**, 309 (2006).
 - [10] T. Blackburn, *Reviews of Modern Plasma Physics* **4**, 5 (2020).
 - [11] L. Pitaevskii, *Sov. Phys. JETP* **12**, 1008 (1961).
 - [12] P. Pershan, *Physical Review* **130**, 919 (1963).
 - [13] J. Van der Ziel, P. S. Pershan, and L. Malmstrom, *Physical review letters* **15**, 190 (1965).
 - [14] T. V. Liseykina, S. V. Popruzhenko, and A. Macchi, *New Journal of Physics* **18**, 072001 (2016).
 - [15] S. V. Popruzhenko, T. V. Liseykina, and A. Macchi, *New Journal of Physics* **21**, 033009 (2019).
 - [16] T. V. Liseykina, A. Macchi, and S. V. Popruzhenko, *The European Physical Journal Plus* **136**, 170 (2021).
 - [17] D. Papadopoulos, Y. Ayoul, A. Beluze, F. Gobert, D. Mataja, A. Fréneaux, N. Lebas, M. Chabanis, M. Dumergue, P. Audebert, and F. Mathieu, in *High Intensity Lasers and High Field Phenomena* (Optica Publishing Group, 2024) pp. HTu2B-2.
 - [18] J. W. Yoon, Y. G. Kim, I. W. Choi, J. H. Sung, H. W. Lee, S. K. Lee, and C. H. Nam, *Optica* **8**, 630 (2021).
 - [19] <https://www.eli-beams.eu/>.

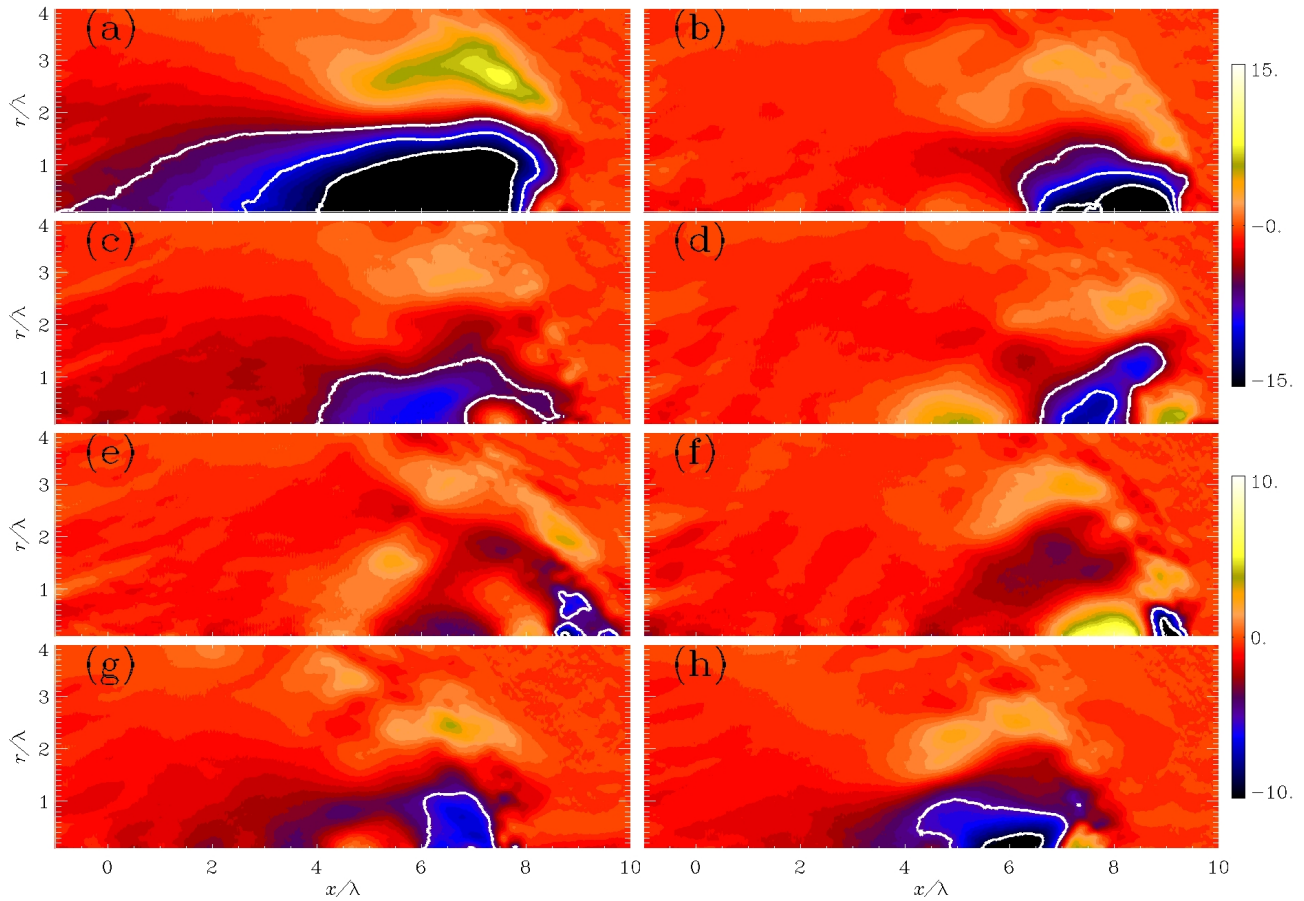


FIG. 3. Magnetic field distribution for the 4-pulse scheme with $2\theta = 5^\circ$ (a,c,e) and $2\theta = 10^\circ$ (b,d,f) calculated at $t = 35T_L$ for the phase shift $\Delta\varphi = 0.0$ (a,b), $\Delta\varphi = 0.2\pi$ (c,d) and $\Delta\varphi = 0.4\pi$ (e,f). The field amplitude $a_0 = 250$ in each beam corresponds to the peak intensity $J \approx 1.4 \cdot 10^{23} \text{W/cm}^2$ and power $P \approx 20 \text{PW}$ per beam. Panel (g) shows the distribution resulting from random relative phase shifts $0.075\pi, -0.018\pi, 0.05\pi$; panel (h) – the distribution for randomly chosen amplitudes $a_0 = 184, 242, 162$ and 239 . The lines of constant magnetic field $B_x = [-15, -10, -5]B_0$ are displayed white.

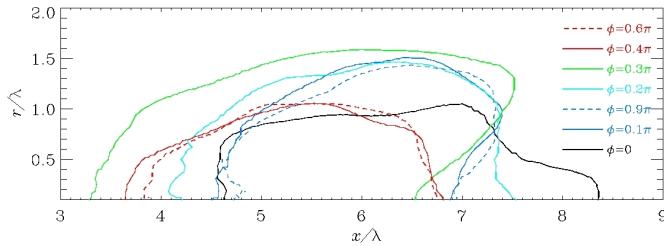


FIG. 4. Lines of constant magnetic field $B_x = -15B_0$ (for $\Delta\varphi < \pi/2$) and $B_x = 15B_0$ (for $\Delta\varphi > \pi/2$) calculated for the 2-pulse scheme at $a_0 = 500$ and $2\theta = 5^\circ$.

[20] D. Doria, M. Cernaianu, P. Ghenuche, D. Stutman, K. Tanaka, C. Ticos, and C. Ur, *Journal of Instrumentation* **15**, C09053 (2020).
 [21] Z. Zhang, F. Wu, J. Hu, X. Yang, J. Gui, P. Ji, X. Liu, C. Wang, Y. Liu, X. Lu, Y. Xu, Y. Leng, R. Li, and Z. Xu, *High Power Laser Science and Engineering* **8**, e4 (2020).

[22] I. Y. Kostyukov, E. Khazanov, A. Shaikin, A. Litvak, and A. Sergeev, *Bulletin of the Lebedev Physics Institute* **50**, S635 (2023).
 [23] V. A. Vshivkov and G. I. Dudnikova, *Computational technologies* **6**, 47 (2001).
 [24] V. A. Vshivkov, N. M. Naumova, F. Pegoraro, and S. V. Bulanov, *Physics of Plasmas* **5**, 2727 (1998), https://pubs.aip.org/aip/pop/article-pdf/5/7/2727/19160381/2727_1_online.pdf.
 [25] T. Liseykina, D. Bauer, S. Popruzhenko, and A. Macchi, in *Proceedings of the International Conference on Example*, NIC Series, Vol. 50, edited by M. Müller, K. Binder, and A. Trautmann, NIC Symposium, Jülich (Germany), 27 Feb 2020 - 28 Feb 2020 (Forschungszentrum Jülich GmbH Zentralbibliothek, Verlag, Jülich, 2020) pp. 405–414.
 [26] J. Derouillat, A. Beck, F. Pérez, T. Vinci, M. Chiaramello, A. Grassi, M. Flé, G. Bouchard, I. Plotnikov, N. Aunai, J. Dargent, C. Riconda, and M. Grech, *Computer Physics Communications* **222**, 351 (2018).
 [27] T. V. Liseykina, E. E. Peganov, and S. V. Popruzhenko, *Bull. Lebedev Phys. Inst.* **50**, S700 (2023).

- [28] K. Yee, IEEE Transactions on Antennas and Propagation **14**, 302 (1966).
- [29] A. B. LANGDON and B. F. LASINSKI, in *Controlled Fusion*, Methods in Computational Physics: Advances in Research and Applications, Vol. 16, edited by J. KILLEEN (Elsevier, 1976) pp. 327–366.
- [30] A. Taflove and S. C. Hagness, *Computational electrodynamics: the finite-difference time-domain method*, 3rd ed. (Artech House, Norwood, 2005).
- [31] Note that the functions in (3) do not solve Maxwell equations, even in the paraxial approximation. Thus, this formula is only used to determine the time dependent boundary condition, while the electromagnetic field in the interaction volume is found by solving the Maxwell equations numerically.
- [32] V. I. Ritus, Journal of Soviet Laser Research **6**, 497 (1985).
- [33] J. G. Kirk, A. Bell, and I. Arka, Plasma Physics and Controlled Fusion **51**, 085008 (2009).
- [34] T. Blackburn, Physical Review A **109**, 022234 (2024).
- [35] M. Tamburini, F. Pegoraro, A. D. Piazza, C. H. Keitel, and A. Macchi, New Journal of Physics **12**, 123005 (2010).
- [36] E. Gelfer, A. Fedotov, O. Klimo, and S. Weber, Matter and Radiation at Extremes **9** (2024).
- [37] E. Gelfer, A. Fedotov, O. Klimo, and S. Weber, Physical Review Research **6**, L032013 (2024).